

Short Communication

Study on Mechanical Performance of CoW/ZrO₂ Composite Film Prepared on Q235B steel by Pulse Electrodeposition

Cuijie Zhang*, Wenlong Wang

Henan Institute of Technology, Xinxiang Henan 453000, China

*E-mail: zhangcj_henan@sina.com

Received: 8 December 2021 / *Accepted:* 25 January 2022 / *Published:* 4 March 2022

The pulse plating technology was used to prepare CoW/ZrO₂ composite film on the surface of Q235B steel. The mechanical performance of CoW/ZrO₂ obtained from plating solution with different concentrations of ZrO₂ nanoparticles was investigated. The CoW/ZrO₂ composite film is crystalline and shows Co₃W structures. ZrO₂ nanoparticle has high surface activity and provides a large number of crystal nuclei for the deposition of CoW alloy, which plays a role in grain refinement and directly enhances the hardness and wear resistance of the CoW/ZrO₂ composite film. However, due to aggregation phenomenon of nanoparticle, the mechanical properties of the CoW/ZrO₂ composite film decrease dramatically when the ZrO₂ in the plating solution is 12 g/L. The composite film formed from the plating bath with 9 g/L ZrO₂ has the best wear resistance and surface hardness.

Keywords: Mechanical performance; CoW/ZrO₂ composite film; Wear resistance;

1. INTRODUCTION

Alloy films possess better physical and chemical performance than single metal film. Compared with single metal film, alloy films often have higher hardness, better wear resistance, more excellent corrosion resistance and so on. Along with the development of material science, alloy films are starting to be used in many fields, such as machinery industry, aviation, manufacturing, magnetic devices and so on [1-5]. Cobalt metal is considered as an important raw material for the production of heat resistant alloys, wear resistance alloys, corrosion resistance alloys and magnetic alloys. Therefore, many cobalt based alloy films with excellent performance have been reported so far [6-10]. For example, CoW alloy films with good corrosion and wear resistance properties were reported by many investigators [11-13]. Some people investigated the performance of CoMo alloy films prepared by chemical or physical method [14-16]. Moreover, CoNi alloy films were also studied and reported in many literatures [17-19]. Although the cobalt based alloy films are extremely reported, it is found out that the performance of cobalt based alloy films could be further improved by doping nanoparticles to

form composite films. For instance, SiC, Al₂O₃ and MoS₂ nanoparticles are beneficial to improve wear and corrosion resistance of cobalt based alloy films which are reported in many papers [20-23]. Electrodeposition is a better way to prepare cobalt based alloy films. However, nanoparticles are easily agglomerated in the solution in the condition of electric field. Therefore, in order to alleviate the agglomeration phenomenon, pulse plating technology is used to obtain CoW/ZrO₂ composite film to greatly improve mechanical properties. The influence of ZrO₂ concentration on thickness, structure, surface morphology, wear resistance of CoW/ZrO₂ composite films was investigated.

2. EXPERIMENTAL

Q235B steel (2 cm×2 cm) was used as the substrate while the pure platinum (3 cm×3 cm) plate was used as the counter electrode. The detail information about the plating solution is listed in Table 1.

Table 1. Composition of plating solution for CoW/ZrO₂ composite film

| Chemical Agent | Concentration (g·L ⁻¹) |
|--|------------------------------------|
| CoSO ₄ ·7H ₂ O | 20 |
| Na ₂ WO ₄ ·2H ₂ O | 10 |
| (NH ₄) ₂ C ₆ H ₆ O ₇ | 100 |
| Na ₂ SO ₄ | 10 |
| H ₃ BO ₃ | 30 |
| ZrO ₂ nanoparticles | 0~12 |

According to Table 1, the Co and W ions were obtained from cobaltous sulfate and sodium tungstate, respectively. Ammonium citrate dibasic was used as the complexing agents. To boost the solution's conductivity, sodium sulfate was used as a conducting salt while boric acid was used as the buffering agent.

The Q235B steel was firstly polished using different grades of sandpapers. Following the polishing of the Q235B steel, 15% NaOH and 10% HCL were employed to remove the oils and oxides from on steel surface. Finally, the substrate was immersed in 100 mL electrolyte to prepare CoW/ZrO₂ composite film by pulse plating at 60 °C for 3600 seconds with continuous stirring. The duty ratio and frequency of pulse plating is 0.5 and 0.025 respectively. The concentration of ZrO₂ particle added in the plating solution ranges from 0 g/L to 12 g/L to investigate the effect of ZrO₂ concentration on mechanical performance of CoW/ZrO₂ composite film.

Cyclic voltammetry curves of CoW electrodeposition were tested by electrochemical station (CHI400C) at the rate of 10 mV/s. The anode was pure plate with 9 cm² while the cathode was Q235B steel with 1 cm². The reference electrode was saturated calomel electrode. Thickness and surface roughness of CoW/ZrO₂ composite film were tested by surface profiler P7 at the condition of 50 μm/s scanning rate and frequency 100 Hz. An X-ray diffraction (Rigaku Ultima) was utilized to examine the

microstructure of the deposited CoW/ZrO₂ composite film, which utilized Cu K α radiation as an incident beam and operated at 40 kV, 150 mA at the rate of 5 degree/min. The hardness of composite film was calculated by Vickers hardness tester (HVS-1000P) at 2.94 N. Friction abrasion meter (HSR-2M) was utilized to evaluate the wear resistance of films at the condition of 5 N load, 6 mm abrasion length and 30 minutes abrasion duration. The surface morphology of CoW/ZrO₂ composite film was observed by scanning electron microscope (SU5000).

3. RESULT AND DISCUSSION

3.1 Electrodeposition mechanism of CoW

Cyclic voltammetry curves of 0.01 M Co²⁺, 0.01 M Co²⁺+0.01 M WO₄²⁻ and 0.01 M WO₄²⁻ were tested respectively shown in Figure 1. As can be seen in Figure 1(2), the typical reduction peak of cobalt could be found at -1.15 V (position b') due to concentration polarization between cathode and bulk solution. Moreover, the cathode current increases sharply at the potential of -0.89 V (position a') which means the cobalt deposition is dominated. The oxidation peak of cobalt is observed at the potential of -0.18 V (position d') which indicates the oxidation of cobalt. The cyclic voltammetry curve of cobalt is investigated by many people [24-26]. The position of reduction and oxidation peak is basically consistent with the experimental results in the paper. Regarding to Figure 1(3), there is no obvious reaction current found on cyclic voltammetry curve of 0.01 M Na₂WO₄ solution which illustrates that tungsten is not able to be deposited directly from aqueous solution. According to the cyclic voltammetry curve of CoW codeposition as Figure 1(1), the cathode current increases extremely at -0.92 V (position a) while the reduction peak appears at -1.09 V (position b).

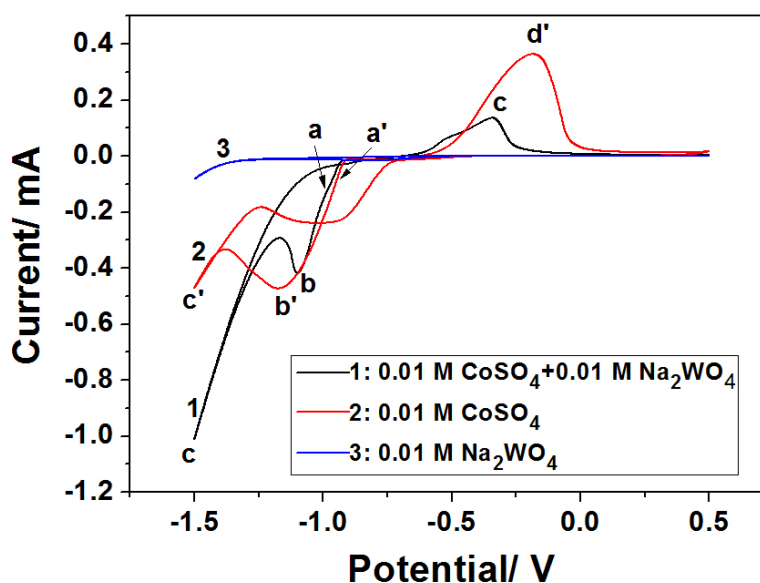
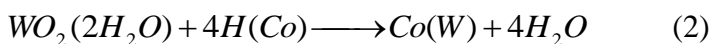
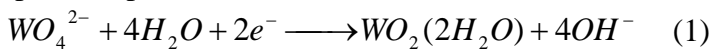


Figure 1 Cyclic voltammetry curves of 0.01 M Co²⁺, 0.01 M Co²⁺+0.01 M WO₄²⁻ and 0.01 M WO₄²⁻ at the rate of 10 mV/s with high voltage 0.5 V and low voltage -1.5 V.

The position of CoW reduction peak is more positive than that of cobalt which means that tungsten ions inhibit the mass transfer of cobalt in the initial stage of electrochemical deposition. The effect of tungsten on electrodeposition process is also reported in many papers [27-29]. However, the cathode current of CoW codeposition at the final potential -1.5 V is almost three times larger than that of cobalt. This phenomenon shows that more metal ions are reduced on the cathode surface indicating the codeposition process of CoW.



The codeposition mechanism of Co and W belongs to a kind of induced codeposition listed in Equation (1) and (2). Tungsten could not be directly deposited from aqueous solution. However, in the presence of cobalt ions, tungstate is reduced to tungsten oxide. Tungsten oxide codeposited with cobalt under the catalytic action of initial hydrogen on the surface of cobalt to form cobalt tungsten alloy. However, some people report that, during the codeposition process of CoW, $[(Co)(HWO_4)(Cit)]^{2-}$ will be formed in the electrolyte to obtain CoW alloys. Different codeposition mechanisms of CoW are investigated in some literatures [30-32].

3.2 Thickness and roughness of CoW/ZrO₂ composite film

The effect of ZrO₂ concentrations on the thickness of CoW/ZrO₂ is shown in Figure 2 and Table 2. It can be seen that the thickness of CoW/ZrO₂ composite film obtained in the experiment belongs to micron scale and the thickness of the composite film obtained varies greatly under the condition of different ZrO₂ concentrations. At the beginning of the experiment, the thickness of composite film increases gradually with the increase of ZrO₂ concentration. CoW/ZrO₂ composite film with maximum thickness (23.69 μm) is obtained when the concentration of ZrO₂ in the bath is 9 g/L.

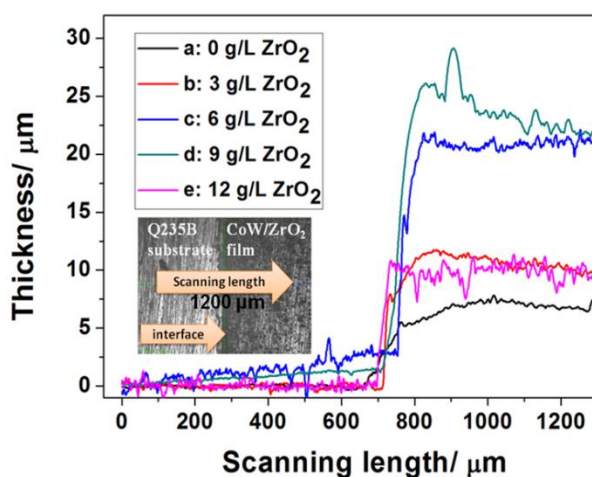


Figure 2. Effect of ZrO₂ concentrations on the thickness of CoW/ZrO₂ composite film

A suitable amount of zirconia nanoparticles continuously gathers on the cathode surface under

the action of agitation, which improves the activity of the cathode surface and increases the nucleation probability resulting in the improvement of thickness. The phenomenon of nanoparticles improves the deposition rate during plating process is introduced in some papers [33-35]. However, too higher ZrO₂ concentration is not conducive to increase the thickness of composite films. When the concentration of ZrO₂ in the bath is 12 g/L, the thickness decreases to 9.25 μm. Due to the excessive suspension of ZrO₂ particles in the plating solution, the active reaction area on the substrate is covered by agglomeration phenomenon, which affects the chemical reaction of cobalt and tungsten, so that the thickness of the film decreases.

Table 2. Thickness of CoW/ZrO₂ composite films

| Sample | ZrO ₂ concentration/ g/L | Thickness/ μm |
|--------|-------------------------------------|---------------|
| a | 0 | 6.48 |
| b | 3 | 11.12 |
| c | 6 | 19.93 |
| d | 9 | 23.69 |
| e | 12 | 9.25 |

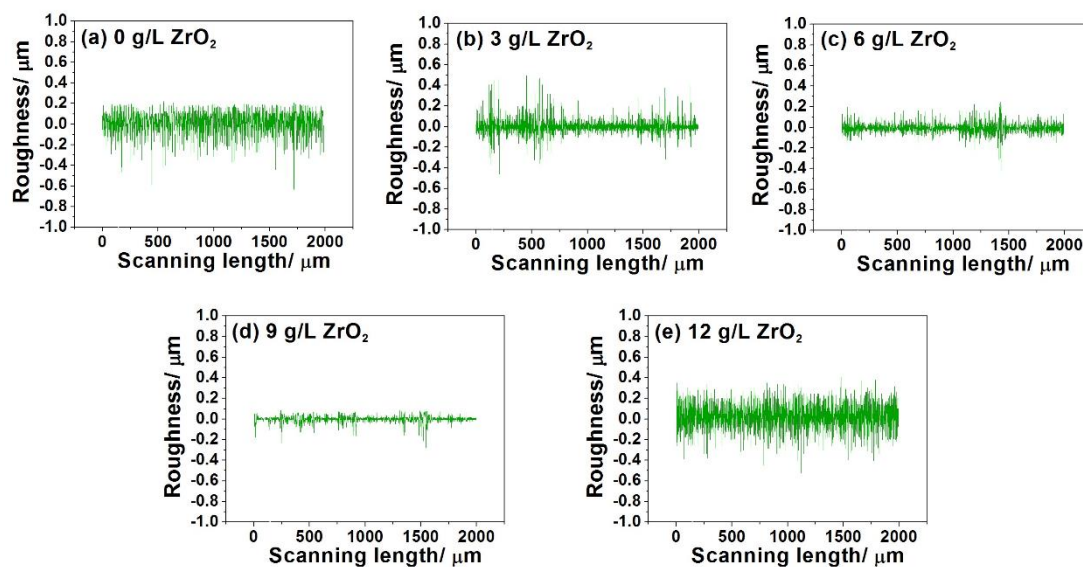


Figure 3. Effect of ZrO₂ concentrations on the roughness of CoW/ZrO₂ composite film

Table 3. Roughness of CoW/ZrO₂ composite films

| Sample | ZrO ₂ concentration/ g/L | Roughness/ μm |
|--------|-------------------------------------|---------------|
| a | 0 | 0.3475 |
| b | 3 | 0.3162 |
| c | 6 | 0.2653 |
| d | 9 | 0.1834 |
| e | 12 | 0.3962 |

Roughness is an important parameter for alloy films. General speaking, the alloy film with lower surface roughness possesses smaller friction coefficient and better wear resistance. The surface roughness of CoW/ZrO₂ composite is listed in Figure 3 and Table 3. With the increase of ZrO₂ concentration, the surface roughness of CoW/ZrO₂ decreases gradually and then increases. The composite film electrodeposited from the solution with 9 g/L ZrO₂ has the lowest roughness, 0.1834 μm. During the plating process, the nano ZrO₂ particle enters into the lattice of CoW alloy and induces heteronucleation, which plays a role in refining grains and reduces the roughness. Nonetheless, the high concentration of zirconia nanoparticles in the plating solution tends to agglomerate near the cathode, which increases the roughness of alloy films.

3.3 Structure and surface morphology of CoW/ZrO₂ composite film

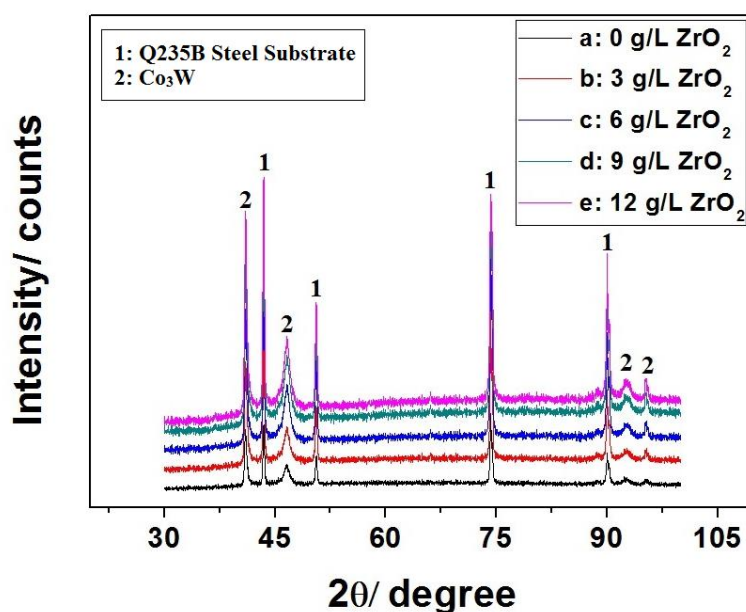


Figure 4. Effect of ZrO₂ concentrations on XRD spectra of CoW/ZrO₂ composite film

Figure 4 displays the XRD patterns of CoW/ZrO₂ composite film prepared from solution containing different ZrO₂ concentrations. According to Figure 4, four peaks marked with 1 stand for the diffraction peaks of Q235B steel substrate. The diffraction peaks of CoW could be observed at $2\theta=40.6^\circ$, $2\theta=46.4^\circ$, $2\theta=91.8^\circ$ and $2\theta=96.5^\circ$ respectively which indicate the structure of Co₃W. This structure is made up of three cobalt atoms and one tungsten atom in a tetrahedral unit. Some researchers also reported the same Co₃W structure [36-37]. When the ZrO₂ concentration in the bath increases from 0 g/L to 9 g/L, the diffraction intensity of Co₃W increases gradually due to the improvement of deposition rate resulting in more crystalline Co₃W structures in the composite film. However, due to different technology parameters, amorphous structure of CoW alloy films have also been prepared and reported [38-39].

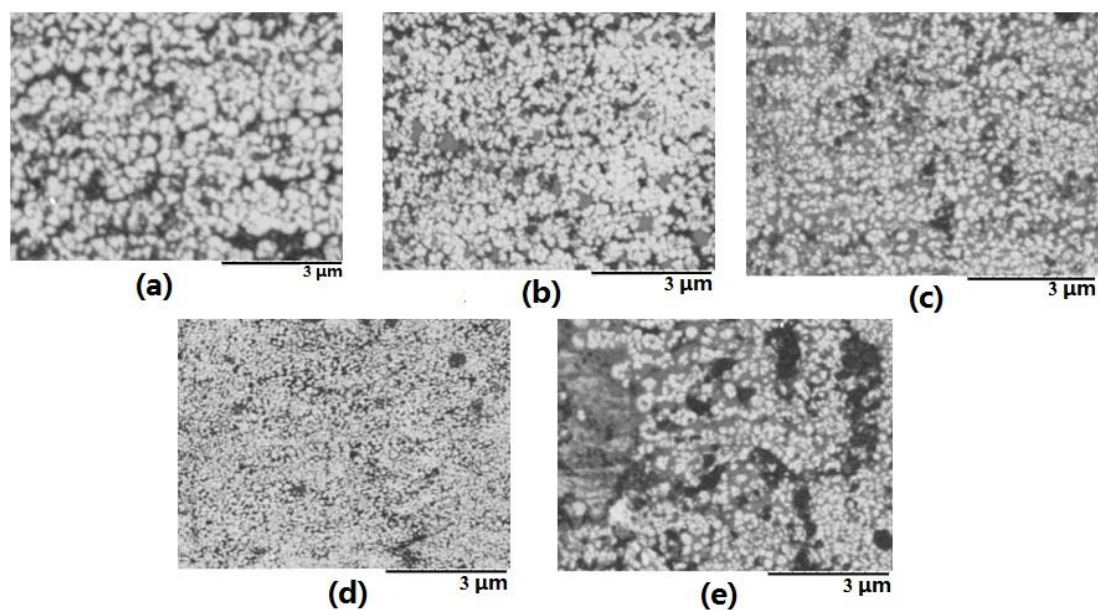


Figure 5. Effect of ZrO_2 concentrations on surface morphology of CoW/ ZrO_2 composite film; (a) 0 g/L ZrO_2 ; (b) 3 g/L ZrO_2 ; (c) 6 g/L ZrO_2 ; (d) 9 g/L ZrO_2 ; (e) 12 g/L ZrO_2 ;

The surface morphology of CoW/ ZrO_2 composite film is shown in Figure 5. It is can be found that different concentrations of ZrO_2 have a certain effect on the surface morphology of the composite film. CoW/ ZrO_2 film presents a typical crystalline particle structure. With the increase of ZrO_2 concentration, the surface particles of the composite film are gradually refined. When the ZrO_2 concentration increases to 12 g/L, the surface of the film becomes loose and roughness due to agglomeration phenomenon of a large amount of ZrO_2 nanoparticles.

3.4 Hardness and wear resistance of CoW/ ZrO_2 composite film

Vickers hardness meter was used to test the hardness of CoW/ ZrO_2 composite film listed in Table 4.

Table 4. Effect of ZrO_2 concentrations on hardness of CoW/ ZrO_2 composite film

| Sample | ZrO_2 / g/L | F/ N | D/ mm | HV |
|--------|---------------|------|--------|-------|
| a | 0 | 2.94 | 0.0399 | 349.2 |
| b | 3 | 2.94 | 0.0375 | 395.3 |
| c | 6 | 2.94 | 0.0357 | 436.2 |
| d | 9 | 2.94 | 0.0321 | 539.5 |
| e | 12 | 2.94 | 0.0369 | 418.5 |

It can be seen from Table 3, the ZrO_2 particles added in the solution is beneficial to improve the surface hardness of CoW/ ZrO_2 composite film. The nano ZrO_2 particle is able to enter into the lattice

of Co₃W tetrahedron structure resulting in the decrease of surface roughness and refining of grain size to greatly improve hardness. The CoW/ZrO₂ composite film obtained from the bath with 9 g/L nano ZrO₂ particle has the best surface hardness equal to 539.5 HV. When 12 g/L ZrO₂ nanoparticles are added into the plating solution, the agglomeration of nanoparticles cover the active area near the cathode to form loose surface morphology with higher roughness leading to the decrease of hardness.

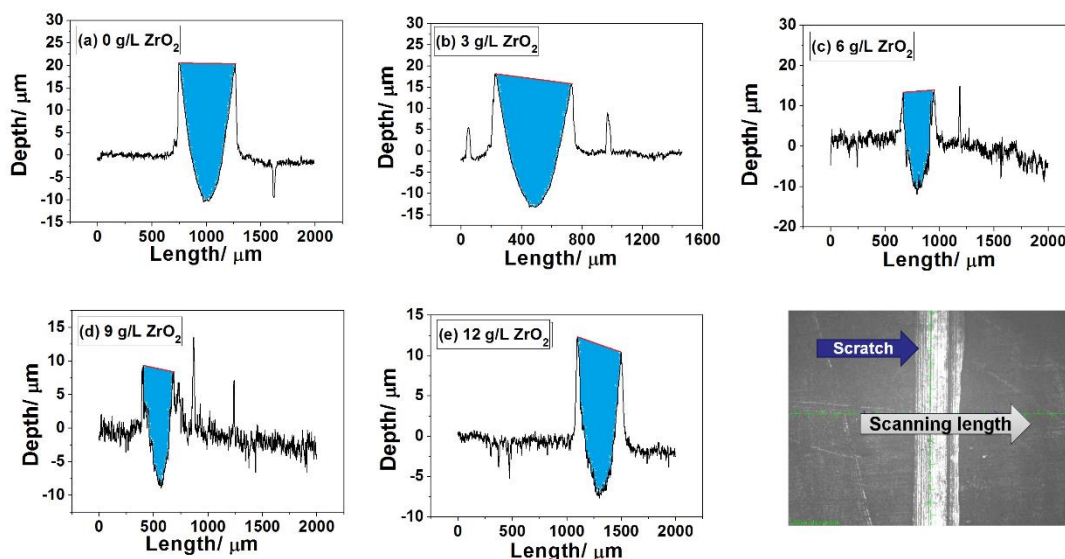


Figure 6. Effect of ZrO₂ concentrations on wear resistance performance of CoW/ZrO₂ composite film

Table 5. Wear parameters of CoW/ZrO₂ composite film

| Sample | ZrO ₂ / g/L | Depth/ μm | Wear area/ μm ² | Wear volume/ mm ³ |
|--------|------------------------|-----------|----------------------------|------------------------------|
| a | 0 | 30.79 | 10122.8 | 0.0607 |
| b | 3 | 29.39 | 9727.2 | 0.0584 |
| c | 6 | 20.76 | 4452.7 | 0.0267 |
| d | 9 | 17.31 | 2930.2 | 0.0176 |
| e | 12 | 22.89 | 4940.1 | 0.0296 |

The scratch with 6 mm length is formed on the surface of composite film after the friction wear testing. The surface profiler is used to measure the depth, sectional area and volume of the scratch to evaluate the wear resistance as shown in Figure 6 and Table 5. The wear volume of CoW alloy film without ZrO₂ particles doping is about 0.0607 mm³ with 30.79 μm depth. When ZrO₂ nanoparticles are introduced during plating process, the wear volume and scratch depth of composite film obviously decrease. It is found out that, the CoW/ZrO₂ composite film obtained from the plating solution containing 9 g/L ZrO₂ particle possesses the smallest wear volume which is only 30% of that of CoW, indicating optimal wear resistance. In the electrodeposition process, ZrO₂ nanoparticle has high surface

activity and provides a large number of crystal nuclei for the deposition of CoW alloy, which plays a role of grain refinement and directly enhances the hardness and wear resistance of the CoW/ZrO₂ composite film. The ZrO₂ nanoparticle is beneficial to improve physical and chemical performance of alloy film prepared by electrodeposition which is also reported by some researchers [40-41]. However, the wear resistance of composite film decreases extremely due to agglomeration phenomenon when the ZrO₂ in the bath is 12 g/L.

4. CONCLUSION

CoW/ZrO₂ composite film was prepared on the surface of Q235B steel by pulse plating technology. The effect of ZrO₂ concentration on thickness, surface roughness, microstructure, wear resistance and hardness of the composite film was investigated. The CoW/ZrO₂ composite film fabricated by pulse plating shows Co₃W structure. It is found that adding proper amount of ZrO₂ in the bath can increase the film thickness, improve the surface hardness, and reduce the wear ratio and roughness of the composite film. The main reason is that ZrO₂ nanoparticle covers the surface of the alloy and can enter into the lattice of CoW alloy to induce heteronucleation, which plays a role in refining grains and enhancing mechanical properties. When ZrO₂ concentration is larger than 12 g/L, due to the agglomeration of nanoparticles, the electrical deposition is inhibited, which contributes directly to the decrease of wear resistance and hardness.

References

1. N. Kilinc, S. Sanduvac and M. Erkovan, *J. Alloy Compd.*, 892 (2022) 162237.
2. Z. Wang, C. Wang, Y. L. Zhao, J. J. Kai, C. T. Liu and C. H. Hsueh, *Vacuum*, 189 (2021) 110249.
3. J. Mitra, A. Kavalur, N. T. Kumbhar, S. Majumdar, N. Das and A. Arya, *Surf. Coat. Technol.*, 404 (2020) 126548.
4. M. R. Karim, D. Panda, A. Adhikari, P. Sharangi, P. Mandal, S. Ghosh, S. Bedanta, A. Barman and L. Sarkar, *Mater. Today Commun.*, 25 (2020) 101678.
5. Y. D. Yu, X. X. Zhao, M. G. Li, G. Y. Wei, L. X. Sun and Y. Fu, *Surf. Eng.*, 29 (2013) 743.
6. E. V. Khomenko, E. E. Shalyguina and N. G. Chechenin, *J. Magn. Magn. Mater.*, 316 (2007) 451.
7. V. Georgescu and M. Daub, *Surf. Sci.*, 600 (2006) 4195.
8. T. E. Bahraoui, H. Errahmani, Y. Belghazi, A. Berrada, A. Dinia, G. Schmerber, H. Lassri and F. Hajji, *J. Magn. Magn. Mater.*, 316 (2007) 8.
9. H. W. Chang, Y. H. Chien, C. Y. Shen, F. T. Yuan, Y. L. Lai, C. R. Wang, L. Horng and W. C. Chang, *Surf. Coat. Technol.*, 398 (2020) 126098.
10. Y. D. Yu, G. Y. Wei, L. Jiang and H. L. Ge, *Int. J. Electrochem. Sci.*, 15 (2020) 1108.
11. S. M. S. I. Dulal, C. B. Shin, J. Y. Sung and C. K. Kim, *J. Appl. Electrochem.*, 38 (2008) 83.
12. A. N. K. Jadoon and M. Z. Khan, *Surf. Eng.*, 26 (2010) 497.
13. Y. D. Yu, J. W. Lou, W. Li, L. X. Sun, H. L. Ge and G. Y. Wei, *Mater. Sci. Tech.*, 28 (2012) 448.
14. E. Gomez, E. Pellicer and E. Valles, *Surf. Coat. Technol.*, 197 (2005) 238.
15. V. V. Kuznetsov, Y. D. Gambur, V. V. Zhulikov, V. M. Krutskikh, E. A. Filatova, A. L. Trigub and O. A. Belyakova, *Electrochim. Acta*, 354 (2020) 136610.
16. C. Li, W. Meng, G. J. Hu, Y. Wang, Z. Q. Cao and K. Zhang, *Int. J. Hydrogen. Energ.*, 43 (2018) 17664.

17. S. Thanikaikarasan, R. Kanimozhi, M. Saravannan and R. Perumal, *Mater. Today: Proc.*, 46 (2021) 10248.
18. P. Cojocar, M. Spreafico, E. Gomez, E. Valles and L. Magagnin, *Surf. Coat. Technol.*, 205 (2010) 195.
19. C. B. Wang, D. L. Wang, W. X. Chen and Y. Y. Wang, *Wear*, 253 (2002) 563.
20. T. Wang, X. Q. Zuo, Y. Zhou, J. H. Tian and S. J. Ran, *J. Mater. Res. Technol.*, 13 (2021) 1615.
21. A. Sharma and B. Ahn, *Appl. Surf. Sci.*, 550 (2021) 149335.
22. Y. Zhou, F. Q. Xie, X. Q. Wu, W. D. Zhao and X. Chen, *J. Alloy Compd.*, 699 (2017) 366.
23. X. H. Zhang, J. J. Liu and B. L. Zhu, *Wear*, 157 (1992) 381.
24. Y. D. Yu, Z. L. Song, H. L. Ge, G. Y. Wei and L. Jiang, *Int. J. Electrochem. Sci.*, 10 (2015) 4812.
25. A. Krause, C. Hamann, M. Uhlemann, A. Gebert and L. Schultz, *J. Magn. Magn. Mater.*, 290 (2005) 261.
26. M. L. Castro, P. Sebastian, M. I. Giannotti, A. Serra and E. Gomez, *Electrochim. Acta*, 359 (2020) 136928.
27. M. Ramaprakash, Y. Deepika, C. Balamurugan, N. Nagaganapathy, R. Sekar, S. K. Panda and N. Rajasekaran, *J. Alloys Compd.*, 866 (2021) 158987.
28. M. H. Allahyarzadeh, M. Aliofkhaezaei, A. S. Rouhaghdam, V. Torabinejad, H. Alimadadi and A. Ashrafi, *Electrochim. Acta*, 258 (2017) 883.
29. Y. S. Yapontseva, T. V. Maltseva, V. S. Kublanovsky and O. A. Vyshnevskiy, *J. Alloy Compd.*, 803 (2019) 1.
30. S. M. S. I. Dual, T. H. Kim, C. B. Shin, and C. K. Kim., *J. Alloys Compd.*, 461 (2008) 382.
31. N. Tsyntsar, H. Cesiulis, A. Budreika, X. Ye, R. Juskenas, and J. P. Celis., *Surf. Coat. Technol.*, 206 (2012) 4262.
32. G. Y. Mukhamedova, M. Ved, N. Sakhnenko and T. Nenastina, *Appl. Surf. Sci.*, 445 (2018) 298.
33. H. Jin, R. J. Ji, T. C. Dong, S. Liu, Y. H. Liu, F. Zhang, C. Ma and S. G. Liu, *Surf. Coat. Technol.*, 421 (2021) 127368.
34. Y. K. Xu, M. Y. Fan, Y. Q. Luo, Y. N. Chen, J. M. Hao and X. H. Hou, *Surf. Coat. Technol.*, 393 (2020) 125797.
35. N. P. Wasekar, L. Bathini, L. Ramakrishna, D. S. Rao and G. Padmanabham, *Appl. Surf. Sci.*, 527 (2020) 146896.
36. M. A. M. Ibrahim, S. S. A. E. Rehim and S. O. Moussa, *J. App. Electrochem.*, 33 (2003) 627.
37. T. Decorps, P. H. Haumesser, S. Olivier, A. Roule and M. Joulaud, *Microelectron. Eng.*, 83 (2006) 2082.
38. G. Abrosimova, N. Volkov, V. Chirkova and A. Aronin, *Mater. Lett.*, 297 (2021) 129996.
39. S. H. Chen, L. Y. Tan, C. L. Yang, P. X. Chen, A. Hu, H. Q. Ling, M. Li and T. Hang, *Mater. Charact.*, 181 (2021) 111448.
40. R. O. Ljeh, C. O. Ugwuoke, E. B. Ugwu, S. O. Aisida and F. L. Ezema, *Ceram. Int.*, 48 (2022) 4686.
41. B. Li and W. W. Zhang, *J. Alloys Compd.*, 820 (2020) 153158.